View Article Online / Journal Homepage / Table of Contents for this issue

Fabrication of hybrid chromophoric amphiphile/silica nanocomposite-based light emitting devices with enhanced performance

Chung-He Yang, Chetan Jagdish Bhongale,* Yung-Ming Liao and Chain-Shu Hsu*

Received 12th September 2006, Accepted 20th October 2006
First published as an Advance Article on the web 9th November 2006
DOI: 10.1039/b613241c

Published on 09 November 2006. Downloaded by National Chiao Tung University on 26/04/2014 08:59:45.

Organic semiconductors show efficient electroluminescence which has led to their commercialization in light-emitting diodes (LEDs), however, they have been marred by the thorniest problem of solid-state quenching. Here, we report the synthesis and characterization of two fluorene-based blue amphiphile emitters containing triphenylamine or anthracene side groups and demonstrate formation of their hybrid meso-structured nanocomposites by sol–gel co-assembly with tetraethyl orthosilicate; and study the molecular interactions within the mesophases formed. The chromophore amphiphiles designed act as photonic active materials as well as structure-directing agents. The new blue luminescent fluorene-based amphiphile/silica co-assembled nanocomposite films have been successfully prepared with enhanced emission. Different kinds of light emitting devices based on these nanocomposites show efficiencies which are improved by several times compared with the corresponding pristine chromophore amphiphiles.

1. Introduction

Since the discovery of devices based on small molecule-derived multilayer structures by van Slyke and Tang[1] and polymeric materials by Friend *et al.*[2] the research in this field has attracted intense attention because of its potential application in display technology. Small molecules and polymer organic light-emitting diodes (OLEDs) bear the promise of revolutionizing display technologies and hence, these devices and the materials that make them functional are the focus of deep scientific and technological interest.[3] Chemistry and chemical principles are central to the evolution of efficient organic light-emitting diodes. Tuning the wavelength or color using different emitting materials, enhancing emission intensity, and controlling constituent physical properties such as solubility and volatility are the areas of focused research involving chemistry. Depending on the role it plays in the OLED, the material has to function either as an efficient charge transporter or an efficient light emitter or sometimes both.[4] Modern OLEDs offer substantial benefits over conventional cathode ray tubes and liquid crystal displays and are predicted to transform the display industry.[3]

Recent development in the organic-templated growth of materials gave rise to new types of photonic hybrid composites whose structure and function are organized hierarchically. Such hierarchically ordered hybrid materials permit the accommodation of a maximum of elementary functions of each participating species in a small volume as small as nanoscale, thereby optimizing properties between the organic and inorganic components and this can be achieved through sol–gel chemistry or self-assembly routes. Such materials with ordered, periodic mesoscopic architecture allow the construction of composites with many types of guests, such as organic specialty molecules or polymers. Over the past several years, there has been a dramatic increase in the literature of design, synthesis, characterization, structure–property studies of zeolites and molecular sieve based composites for catalysis and optical applications. In addition to metal and metal oxide clusters embedded in the pores of host materials, the encapsulation of organic dye molecules and metal organic compounds has gained particular attention.[5] The preparation methods, properties, and possible applications of chromophores in porous silica and molecular sieves have been summarized in a recent review article.[6] Schulz-Ekloff's group has demonstrated inclusion of dye molecules such as Coumarin 40, Rhodamine BE50, or Oxazine 1 inside the nanopores[5,7,8] and several papers on this topic showed the optimization of the concentration of dye molecules within preformed mesopores or during sol–gel synthesis. These composite materials showed an increase in photoluminescence intensity at moderate dye concentrations.[9–11] Surfactant template-directed self-assembly of nanosize pores in silica thin films is increasingly being used to make photoresponsive materials.[12–15] Self-assembly typically employs nonsymmetric molecules that are programmed to organize into well-defined supramolecular assemblies.[14] Amphiphilic surfactant molecules or polymers bearing hydrophilic and hydrophobic parts are the most common examples. Sol–gel synthesis of mesoporous silica with functional templates has attracted attention for the fabrication of nanocomposite materials, because this method, in contrast with statistical postloading approaches, guarantees dense filling of organic functional groups in the silicate channels.[16] Stable, supported films prepared by this method can be processed into porous or composite mesostructures with potential utility for a variety of applications such as membranes,[17] sensors,[18] lasers,[5,19,20] waveguides,[19]

Department of Applied Chemistry, National Chiao Tung University, 1001, Ta-Hsueh Road, Hsinchu 30010, Taiwan, R.O.C. E-mail: chetan.ac90g@nctu.edu.tw; Fax: +886-3-5723764; Tel: +886-3-5131523

View Article Online

Published on 09 November 2006. Downloaded by National Chiao Tung University on 26/04/2014 08:59:45.

low-dielectric-constant (low k) insulators,[21,22] *etc*. Okabe *et al.* have demonstrated the immobilization and tuning of one-dimensional, columnar, charge-transfer (CT) assemblies in mesoporous silica films consisting of hexagonal array of nanoscopic channels.[23] The fabrication and characterization of multiply doped nanostructured silicate sol–gel thin films has also been reported by Zink's group.[24,25] Previously, we have demonstrated the preparation of chromophore amphiphile/silica self-assembled nanocomposites with enhanced emission.[26] The fabrication of thin layers is essential for many technical applications and for this the molecules have to show an ordered structure within these thin films to enhance or even cause certain desired properties. Controlled and well-ordered chromophoric aggregation lead to highly emissive states.[26] Here, we report the synthesis and characterization of two fluorene-based blue amphiphile emitters containing triphenylamine or anthracene side groups as the hydrophobic part and two long alkyl chains attached to the C-9 carbon of fluorene moiety and hydroxyl head-groups as the hydrophilic part. Organic light emitting devices, with enhanced performance, were fabricated with the nanocomposites formed from the sol–gel co-assembly of these chromophoric amphiphiles with silica precursors. These devices have better efficiencies compared to that fabricated using pristine chromophoric amphiphiles alone.

2. Results and discussion

Synthesis and characterization of the chromophore amphiphiles and their nanocomposites

The chromophore amphiphiles (FL-TPA-$(C11)_2$ and FL-DAN-$(C11)_2$) were synthesized and their formation was confirmed by NMR, mass spectroscopy and elemental analysis data (see Scheme 1 and the Experimental section). The optimized molecular geometries, obtained by minimizing the energy of AM1 calculations (HyperChem 7.5), of these chromophore amphiphiles are shown in Fig. 1b. Triphenylamine (TPA) and anthracene derivatives are well-known blue-light emitting chromophores. Moreover, arylamines are good hole-transport materials having a high hole mobility. They have previously been incorporated into main-chain or side-chain polymers. We therefore introduced a TPA segment into the fluorene moiety and prepared luminescent blue emitter FL-TPA-$(C11)_2$ with hole-transport properties. These two fluorene-based derivatives were designed to be blue light-emitting materials with high photoluminescence (PL) efficiencies. In dilute THF solutions, the external quantum efficiency of FL-TPA-$(C11)_2$ was observed to be 80%, and for FL-DAN-$(C11)_2$ it was 68%. Hybrid nanocomposites of these chromophore amphiphiles with silica precursors were formed by sol–gel co-assembly. Precursor solutions were synthesized from tetraethyl orthosilicate (TEOS, $Si(OC_2H_5)_4$), chromophoric amphiphiles (FL-TPA-$(C11)_2$ or FL-DAN-$(C11)_2$), and HCl catalyst prepared in THF–water solvent. The final reactant mole ratio for nanocomposites prepared from FL-TPA-$(C11)_2$ and FL-DAN-$(C11)_2$, were 1 TEOS : 30 THF : 5 H_2O : 0.1 HCl : 1 chromophoric amphiphile. In a typical preparation, TEOS, THF, water and dilute HCl were stirred and heated at 35 °C for half an hour. To this solution was added the chromophoric amphiphile in THF and the mixture was stirred for three hours. During the addition, a colloidal solution started to form and films were prepared on substrates by spin-coating (1500 rpm), or dip-coating. The co-assembly of chromophore amphiphile/silica micelles led to further organization into ordered mesophases. The chromophore amphiphiles act as photoactive molecules as well as structure-directing agents.

Spectroscopic properties of the nanocomposites

X-Ray diffraction (XRD) analysis of the nanocomposite thin films showed broad and intense single Bragg peaks in the low 2θ region, characteristic of periodic mesoscopic silicate structures, and were around $2\theta = 1.54$ and 1.56° for nanocomposite films of FL-TPA-$(C11)_2$ and FL-DAN-$(C11)_2$, respectively (see Fig. 1a). Similar observations were reported for the hierarchically structured transparent hybrid materials by *in situ* growth of mesostructured organosilica in a host polymer.[27] The reason for the observation of only a single peak may be that the films were drawn after a few hours of the liquid crystal-templated[28] composite formation and so the structures were not fully evolved. TEM images of the nanocomposites revealed that the composite with FL-DAN-$(C11)_2$ has a uniform mesostructure but with no apparent long-range ordering[29] (Fig. 1d), whereas the nanocomposite produced with FL-TPA-$(C11)_2$ displays a highly uniform periodic mesostructure (Fig. 1c); however, this could not be well demonstrated by XRD, as the peaks were only observed in the low 2θ region. The difference in transmission electron microscopy images may be due to the size and orientation of the chromophore groups around the hydrophobic core and the length and the size, consequently the stereochemistry, of the chromophore amphiphiles in the nanocomposites as both these factors affect the topology of amphiphilic molecules and hence the packing of the chromophores within the channels—the bulkier the group is, the greater the steric hindrance and so the looser the packing of the chromophores. We propose that increasing the surfactant tail area, and consequently that of the chromophore, might reduce the value of the surfactant packing parameter (g)[12] and thus affect the mesostructure formation. These factors decide the extent of aggregation of the molecules within the inorganic framework. The present results show that these precursors have the ability to form mesophases by sol–gel co-assembly.

The UV/Vis absorption and photoluminescence (PL) spectra for the FL-TPA-$(C11)_2$ nanocomposite are shown in Fig. 2a and b, respectively. FL-TPA-$(C11)_2$ is an amphiphile consisting of two triphenylamine side groups attached to the fluorene moiety as the hydrophobic part and long alkyl chains with hydroxyl head groups as the hydrophilic part. The absorption band of FL-TPA-$(C11)_2$ in dilute THF solution is observed at 374 nm and was attributed due to a π–π^* transition, but when a thin film of FL-TPA-$(C11)_2$ is formed, its absorption undergoes a red shift of about ten nanometers to 384 nm. The nanocomposite thin film, however, compared to the pristine chromophore amphiphile FL-TPA-$(C11)_2$ film shows a maximum emission peak (λ_{max}) around 374 nm. The absorption peak position for FL-TPA-$(C11)_2$ solution as well as nanocomposite was thus the same. The PL spectrum

 This journal is © The Royal Society of Chemistry 2007

View Article Online

Published on 09 November 2006. Downloaded by National Chiao Tung University on 26/04/2014 08:59:45.

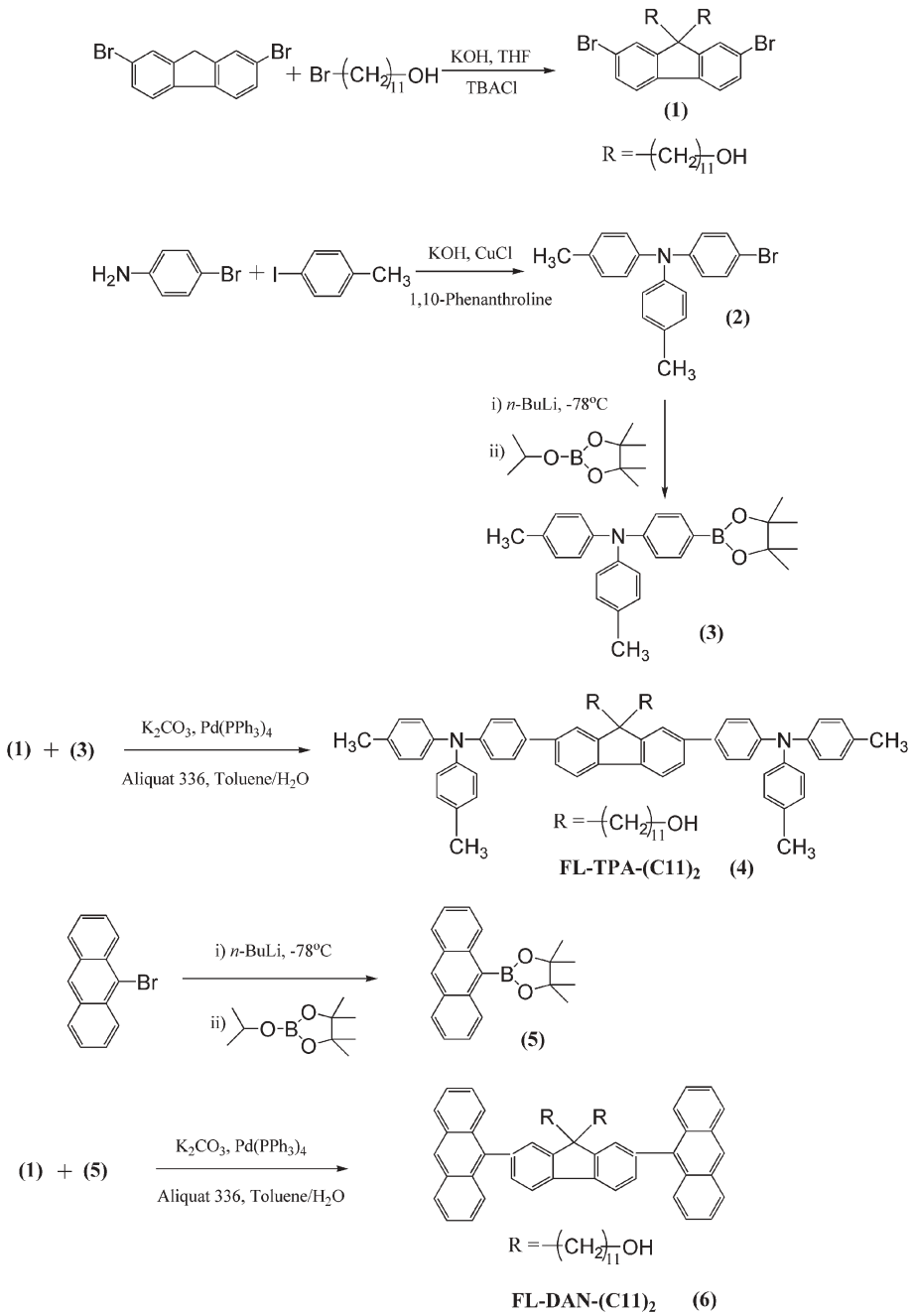

Scheme 1 Synthesis of FL-TPA-$(C11)_2$ and FL-DAN-$(C11)_2$ chromophore amphiphiles.

of FL-TPA-$(C11)_2$ in THF shows a bright blue fluorescence with the peak maximum at about 432 nm. In the solid state its intensity undergoes a large decrease with a fairly large red shift and the maximum peak at about 445 nm was observed. This may be caused by the formation of intermolecular species, *i.e.*, aggregates and/or excimers. However, in the nanocomposite we observe a strong emission enhancement in the blue region, with a maximum peak at 438 nm and a few shoulder peaks, however, not so well-pronounced at higher wavelength were observed. This fluorescence change, with about a six-fold increase in the intensity, is quite unusual considering that the fluorescence efficiency of organic chromophores generally decreases in the solid state, although they show high fluorescence efficiency in solution. This quite general decrease is attributed mainly to intermolecular vibronic interactions, which induce a nonradiative deactivation process—fluorescence quenching—by excitonic coupling, excimer formation, and excitation energy migration to the impurity traps. The emission enhancement observed in the nanocomposite films is due to the well-ordered arrangement of the chromophore groups on the nanoscale. The external quantum efficiency (Φ), as measured by an integrating sphere method, for the FL-TPA-$(C11)_2$ chromophore film is 7.6%, and it increases to 21.5% in the FL-TPA-$(C11)_2$ nanocomposite film.

The other chromophore amphiphile studied, FL-DAN-$(C11)_2$, has a planar chromophore anthracene group

View Article Online

Published on 09 November 2006. Downloaded by National Chiao Tung University on 26/04/2014 08:59:45.

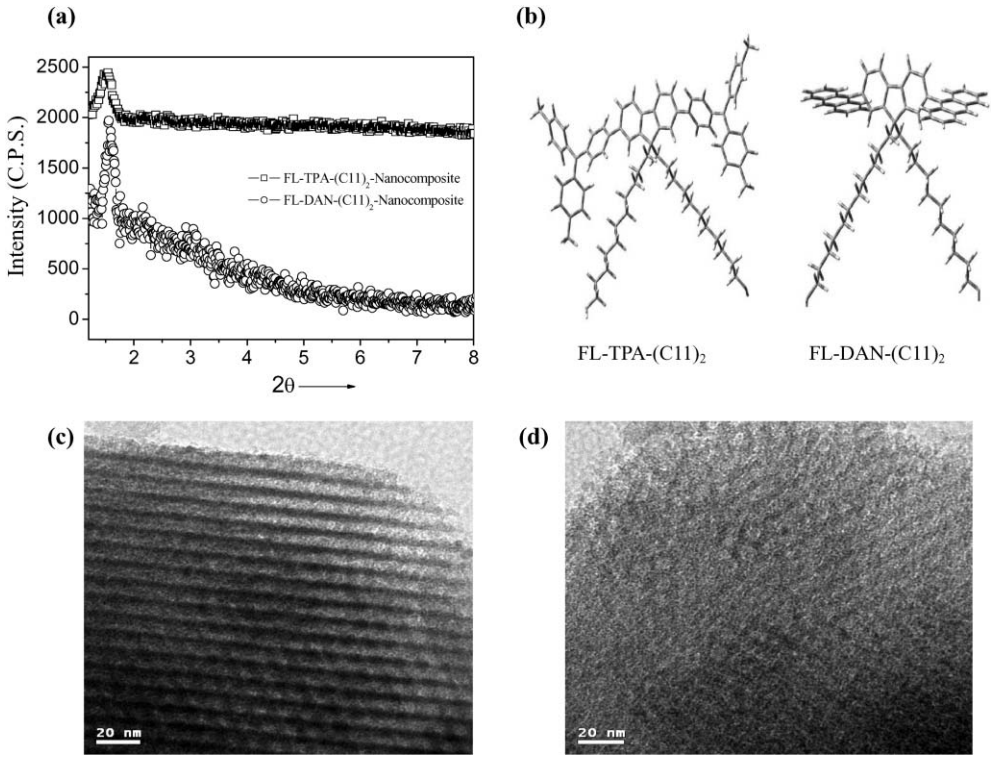

Fig. 1 a) X-Ray diffraction patterns of the mesostructured chromophore amphiphile/silica nanocomposites formed by FL-TPA-$(C11)_2$ and FL-DAN-$(C11)_2$. b) Optimized molecular structures of the chromophore amphiphiles obtained from AM1 calculations. Transmission electron microscopy (TEM) images of the nanocomposites formed by c) FL-TPA-$(C11)_2$ and d) FL-DAN-$(C11)_2$.

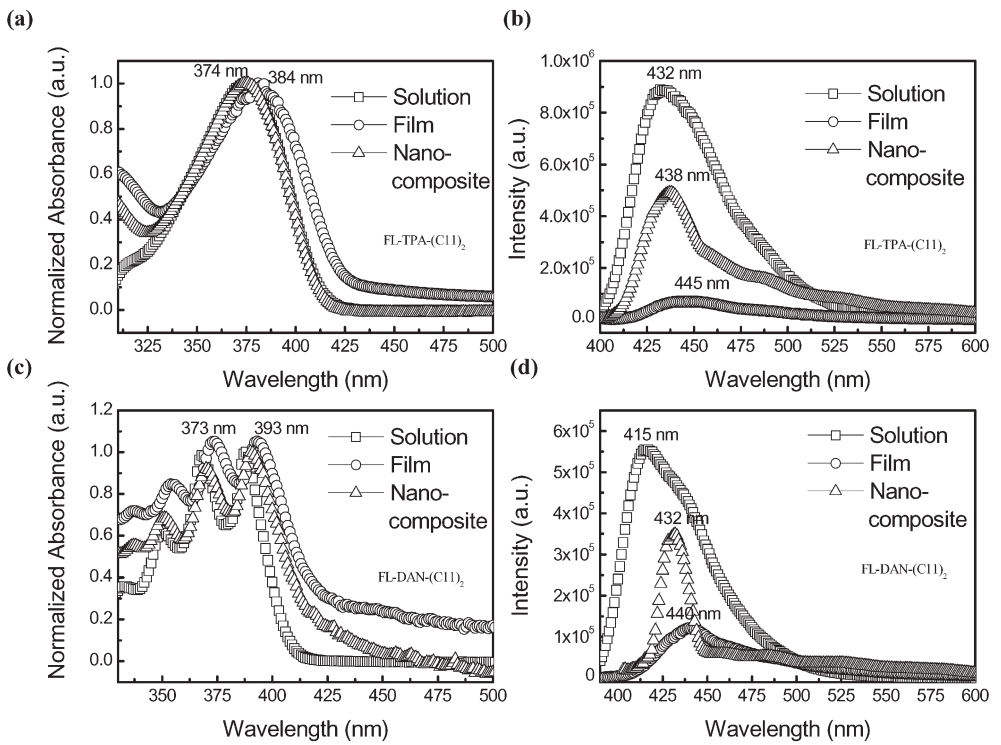

Fig. 2 UV/Vis absorption and PL spectra of FL-TPA-$(C11)_2$ (a, b) and FL-DAN-$(C11)_2$ (c, d) for solution, pristine chromophore amphiphile and nanocomposite films, as indicated. PL intensities of solutions were normalized for comparison.

 This journal is © The Royal Society of Chemistry 2007

View Article Online

Published on 09 November 2006. Downloaded by National Chiao Tung University on 26/04/2014 08:59:45.

(compared to triphenylamine in FL-TPA-$(C11)_2$) attached to the fluorene moiety, as the hydrophobic part and hydroxyl head groups as the hydrophilic part. The dilute THF solution of FL-DAN-$(C11)_2$ shows three clearly resolved absorption bands at 350, 368 and 388 nm, respectively (Fig. 2c). These bands red-shift for the pristine chromophore films by about 4–5 nm (354, 373, 393 nm, respectively). However, the nanocomposite film shows blue-shifted absorption peaks around 351, 370, 390 nm, respectively, compared to the pristine chromophore films; resembling those with solution absorption peaks. FL-DAN-$(C11)_2$ in dilute THF solution shows blue fluorescence with a maximum peak (λ_{max}) at 415 and a shoulder around 432 nm in the PL spectrum (Fig. 2d). In the pristine chromophore amphiphile film the PL intensity is quenched and red-shifted, although it still shows the well-resolved vibronic features with λ_{max} at 440 nm. The large 25 nm red shift is attributed to the more coplanar structure of FL-DAN-$(C11)_2$ that induce strong molecular chain interactions in the film state. However, when the nanocomposite film of FL-DAN-$(C11)_2$ is formed by templated co-assembly, its emission intensity is enhanced about three-fold compared to the pristine chromophore amphiphile film alone, with λ_{max} at 432 nm. The external quantum efficiency (Φ) for the FL-DAN-$(C11)_2$ chromophore film is 5%, and it increased up to 30% in the FL-DAN-$(C11)_2$ nanocomposite films. The 'controlled' aggregation of the chromophore groups within the hydrophobic core of the nanocomposite minimizes the formation of larger crystals and thus enhances the fluorescence. The nanopackets in the hybrid composites could provide a controlled concentration of active dots or chromophores, which are better well-defined systems, and could prevent coalescence into larger, ill-defined aggregates.[26] Although Forster quenching is observed in most cases for fluorescent molecules in molecular sieves, the fluorescence enhancement induced in this case is attributed to the well-ordered nanopackets of "controlled" chromophore aggregates formed in the co-assembled nanocomposites, as is evident from the above results. Moreover, recent studies[26,30,31] on the aggregation-induced emission (AIE) enhancement for a diverse range of conjugated organic nanoparticles show that organic nanoparticles have special properties that lie between the properties of molecules and those of bulk materials and this is well exploited here to form the mesostructured thin films by sol–gel co-assembly of the chromophore amphiphile nanoaggregates. The steric interactions of the chromophores or amphiphiles all have an effect on the optical properties. In these nanocomposites, the chromophore molecules were surrounded by a silica framework restricting the intermolecular aggregation, thus contributing to the sterically controlled, ordered orientation of the chromophore amphiphiles. We anticipate that the three-dimensional structures of the chromophore amphiphiles (see Fig. 1b) would restrict close packing of the molecules and reduce any intermolecular π–π interactions and, consequently, suppress aggregate/excimer formation and enhance the photoluminescence quantum efficiency. The intensity increase may be due to an increased quantum efficiency of the chromophore nanoaggregates within silica. Such a fluorescence enhancement has also been observed for the well-packed conjugated polymer[32] chains and aggregates and for fullerene aggregates in hybrid nanocomposites.[9] Energy optimization of the two chromophore amphiphiles using B3LYP density functional theory suggests that the angle between the planes of the anthracene and fluorene moieties is about 102° and that between fluorene and the adjacent benzene ring of the TPA is about 38°. Anthracene is planar whereas triphenylamine is three-dimensional. Owing to the planar structure of anthracene segments in FL-DAN-$(C11)_2$, the aggregation of the molecular chains may be increased as compared to that in the FL-TPA-$(C11)_2$ nanocomposite and so there are differences in the PL intensities of these nanocomposites and this will be discussed further with regards to the device performance in the following section.

Cyclic voltammetry

The electrochemical behaviors of these two chromophoric nanocomposites were investigated by cyclic voltammetry (CV) (see Fig. 3a and b). The corresponding highest-occupied molecular orbital (HOMO) and lowest unoccupied molecular orbital (LUMO) energy levels were estimated from the onset of the redox potentials. HOMO and LUMO levels of the chromophores were calculated according to the empirical formulae $E_{HOMO} = -(E_{ox} + 4.4)$ (eV) and $E_{LUMO} = -(E_{red} + 4.4)$ (eV). From the difference of the onset potentials and the optical band gaps (E_g) calculated from the onsets of the UV-vis absorption spectra, the energy levels, the oxidation and reduction potentials were determined and are summarized in Table 1, and the band diagrams of FL-TPA-$(C11)_2$ and FL-DAN-$(C11)_2$ nanocomposites are shown in Fig. 4a.

It can be seen that both FL-TPA-$(C11)_2$ and FL-DAN-$(C11)_2$ possess similar electrochemical properties like those of the fluorene moiety. The reversible oxidation curves of the molecules with onsets around 1.00 and 1.47 eV could be assigned to the p-doping oxidation potential of the fluorene segment.[33] The reversible oxidation wave with onset at around

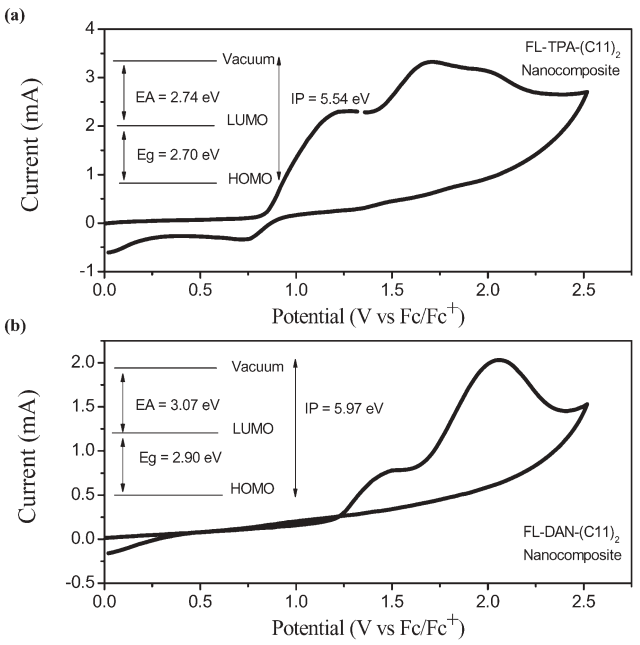

Fig. 3 Cyclic voltammograms of the nanocomposites formed by a) FL-TPA-$(C11)_2$ and b) FL-DAN-$(C11)_2$ amphiphiles.

View Article Online

Published on 09 November 2006. Downloaded by National Chiao Tung University on 26/04/2014 08:59:45.

Table 1 Electrochemical properties of FL-TPA-$(C11)_2$ and FL-DAN-$(C11)_2$ nanocomposites

Nanocomposite	Optical band gap/eV[a]	E_{ox}/eV[b]	E_{red}/eV[b]	HOMO/eV[c]	LUMO/eV[c]
FL-TPA-$(C11)_2$	2.89 (429)	1.01	−1.88	−5.41	−2.52
FL-DAN-$(C11)_2$	2.90 (428)	1.47	−1.43	−5.87	−2.97

[a] The optical band gap estimated from the onset wavelength (value in parentheses) of UV/Vis absorption spectra of the nanocomposite film. [b] The E_{ox} and E_{red} are the onset potentials of oxidation and reduction, respectively. [c] Calculated from the empirical formulae: $E_{(HOMO)} = -(E_{ox} + 4.40)$ (eV), $E_{(LUMO)} = -(E_{red} + 4.40)$ (eV).

0.83 eV and the higher HOMO levels for FL-TPA-$(C11)_2$ (−5.41 eV) might originate from the electron-rich nature of the TPA moiety and are similar to what has been reported for TPA-substituted polyfluorene (−5.34 eV).[34] Notice the HOMO level of FL-DAN-$(C11)_2$ is 5.87 and this lower value forms a large energy gap for the hole to transport in a LED device. So the device performance is not so good for FL-DAN-$(C11)_2$, and this will be further discussed in the electroluminescence section.

Device fabrication and characterization

To evaluate the EL performance of chromophore amphiphiles in this study, three different device architectures were designed and fabricated. For comparison purposes, device A was designed in a double-layer structure of ITO/PEDOT : PSS/EML/Ca/Al configuration. Device B is a blue device incorporating the novel crosslinkable hole transport layer PCF11 (20 nm) along with an emitting layer (EML) and can be shown as ITO/PEDOT : PSS/PCF11/EML/Ca/Al. Device C is also a blue device with TPBI (as electron transport layer (ETL)) inserted between the emission layer (EML) and the cathode and can be shown as ITO/PEDOT : PSS/EML/TPBI/Al. The emitting layer (EML) was either the chromophore amphiphile or its nanocomposite and was deposited by spin-coating. The general device architecture and molecular structures of PCF11 and TPBI (1,3,5-tris(2-*N*-phenylbenzimidazolyl)benzene) are shown in Fig. 3b and c, respectively. Poly(3,4-ethylenedioxythiophene) (PEDOT) is the hole-injecting layer and Ca/Al is the bilayer cathode. In device B, PCF11 was deposited on PEDOT by spin-coating from toluene and then crosslinking the films by irradiation with 302 nm light for 1 min at room temperature. It is worth noting that further depositing the emitting layer by spin-coating does not dissolve the PCF11 layer. The highest occupied molecular orbital (HOMO) of PCF11 (5.33 eV), which is higher than those for the FL-TPA-$(C11)_2$ (5.41 eV) and FL-DAN-$(C11)_2$ (5.87 eV) nanocomposites, together with PEDOT make up the hole-transport layer and improve the device performance. In device C, a thin TPBI layer (30 nm) was used as ETL, which also functions as a hole-blocking layer at the cathode side.

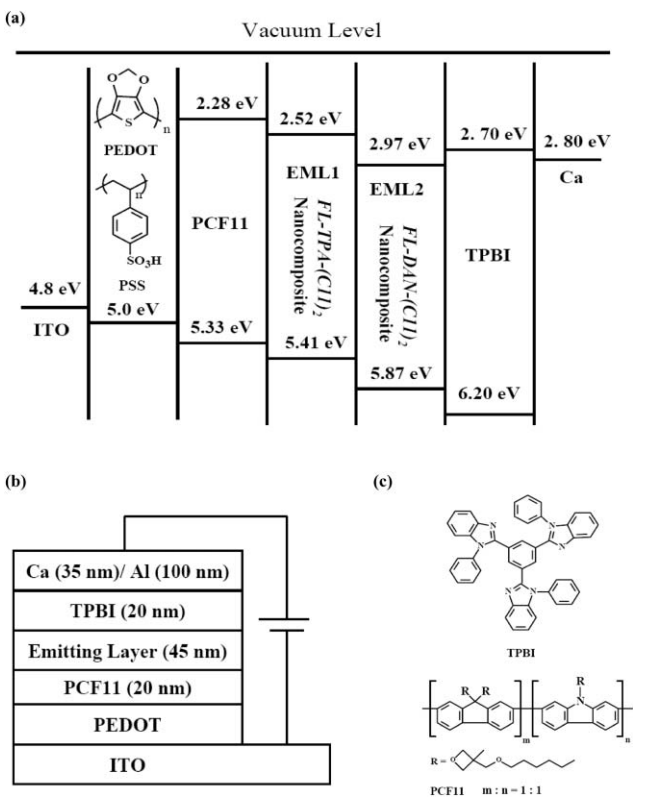

Fig. 4 a) Schematic illustration of the energy level diagram. b) Schematic illustration of the general device architecture of the light emitting devices fabricated. PEDOT and PCF11 make hole-transport layers (HTL), the hybrid nanocomposite of FL-TPA-$(C11)_2$) or FL-DAN-$(C11)_2$ is the emitting layer and TPBI is the electron transport layer; ITO is indium tin oxide and Ca/Al is the bilayer cathode. c) Molecular structures of PCF11 and TPBI.

Fig. 5a and b show the typical EL spectra of the devices A fabricated using the nanocomposite films of chromophore amphiphiles FL-TPA-$(C11)_2$ and FL-DAN-$(C11)_2$, respectively, along with their PL spectra. Small luminescent molecules tend to aggregate in the film state accompanied by a red-shifted and less efficient luminescence. The broad electroluminescence (EL) curve of pristine FL-TPA-$(C11)_2$ (spin-coated from 5% THF solution) around 400–600 nm is attributed to ill-defined aggregate formation of the chromophore molecules. The EL $CIE_{x,y}$ coordinates at 14 V for this material lie in the green region at (0.28, 0.37). However, for the FL-TPA-$(C11)_2$ nanocomposite, its EL peak at 428 nm is identical to that of its PL spectrum. No undesirable excimer/aggregate emission was observed at a longer wavelength like that observed for the pristine molecule. This also suggests that the sol–gel co-assembly of the chromophore amphiphiles with TEOS would form well-organized mesoscopic structures and avoid the coalescence of ill-defined aggregates of the chromophores. Pristine FL-DAN-$(C11)_2$, on the other hand, does not show electroluminescence and this is attributed to the probable formation of ill-defined aggregates or excimers due to the planar structure of the anthracene moiety. Moreover, both of these chromophore amphiphiles were deposited by the spin-coating method instead of vapor deposition; and this may have caused bad film formation. However, electroluminescence could be observed in the case of the FL-DAN-$(C11)_2$

 This journal is © The Royal Society of Chemistry 2007

View Article Online

Published on 09 November 2006. Downloaded by National Chiao Tung University on 26/04/2014 08:59:45.

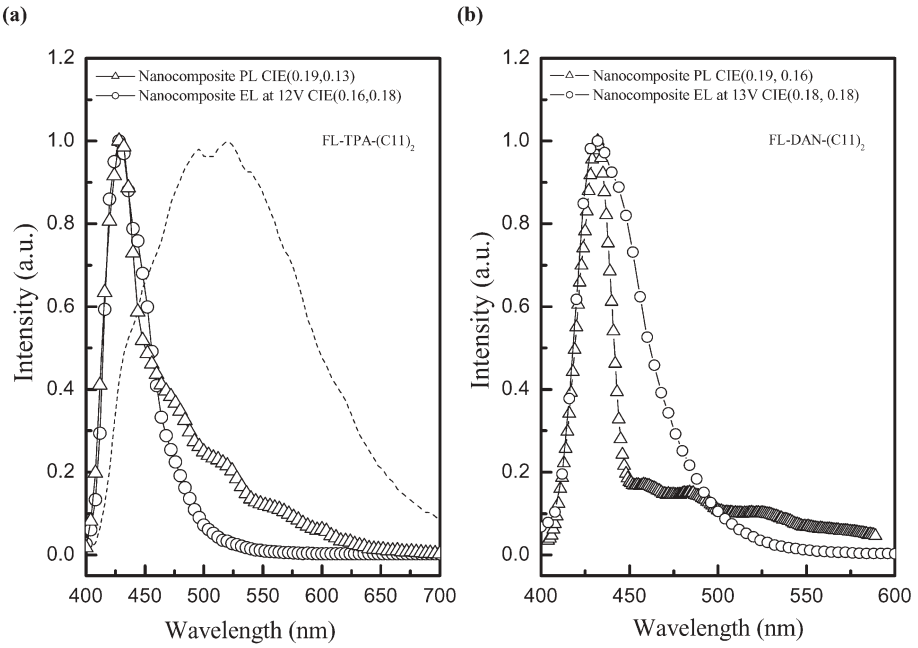

Fig. 5 a) EL and PL spectra of the nanocomposite of chromophore amphiphile FL-TPA-$(C11)_2$. EL of pristine FL-TPA-$(C11)_2$ film at 12 V CIE (0.28, 0.37) (dashed line) is shown for comparison. b) EL and PL spectra of the nanocomposite of chromophore amphiphile FL-DAN-$(C11)_2$.

nanocomposite. The peak maxima for the nanocomposite EL and PL spectra were identical, *viz.* 432 nm. It is worth noting that in most small molecule devices, vacuum deposition is necessary because small molecules possess bad film-forming properties; however, co-assembly with silica facilitates good film formation and retains the emission properties of the single chromophore.

The EL performances of FL-TPA-$(C11)_2$ and FL-DAN-$(C11)_2$ and their nanocomposites are summarized in Table 2. Fig. 6 shows a comparison of the current density–voltage, luminescence–voltage and yield–voltage characteristics of the devices prepared, as indicated. The highest occupied molecular orbital (HOMO) of PCF11 (5.33 eV) has been shown to transport holes in the FL-TPA-$(C11)_2$ nanocomposite resulting in a higher current density (Fig. 6a). However, for the FL-DAN-$(C11)_2$ nanocomposite, the HOMO level between the PCF11 and the emitting layer is still too large to overcome and moreover the higher LUMO level of PCF11 (2.28 eV) may effectively block electrons from reaching the HTL resulting in the lower current density (Fig. 6d). We found that the luminescence (L) of device B could be significantly enhanced from 247 to 588 cd m^{-2} (Fig. 6b) when PCF11 is used as HTL for the FL-TPA-$(C11)_2$ nanocomposite. Device B achieves an EL efficiency of 0.18 cd A^{-1} at 12 V (Fig. 6c) and this dramatic increase in EL, by about four-fold compared to that of the nanocomposite in device A, can be attributed to the formation of a narrow recombination zone in which both the charge carriers and the excitons are confined by the electron-blocking layer PCF11. This new hole-transport layer provides a more effective pathway for hole injection and balances the hole and electron carriers arriving at the recombination zone. In device C, with the introduction of TPBI as the electron transport and hole-blocking layer, the EL efficiency could be significantly enhanced from 0.04 to 0.12 cd A^{-1}. In Fig. 6a, the current densities of nanocomposites in devices B and C were lower than that in device A at higher voltage. The luminescence for device B was increased significantly compared to that for device A. This suggests that the PCF11 and TPBI layers effectively block the electrons and holes, respectively, further improving the device efficiency. The different turn-on voltages for FL-TPA-$(C11)_2$ pristine (7 V) and nanocomposite (10 V) are attributed to the thickness of the emitting layers. The low turn-on voltage of the nanocomposite film clearly demonstrates that the silica component inside is not the main cause influencing the turn-on voltage, but the thickness of the film is. As mentioned above, the pristine FL-DAN-$(C11)_2$

Table 2 The EL performance of the three types of devices made from FL-TPA-$(C11)_2$ and FL-DAN-$(C11)_2$ nanocomposites

Emitting layer	Device structure	L_{max}/cd m^{-2}	$Yield_{max}$/cd A^{-1}	CIE 1931 (x,y)
FL-TPA-$(C11)_2$ (pristine)	Type A	61	0.04	0.28, 0.37
FL-TPA-$(C11)_2$ (nanocomposites)	Type A	247	0.05	0.16, 0.18
FL-TPA-$(C11)_2$ (nanocomposites)	Type B	588	0.18	0.17, 0.18
FL-TPA-$(C11)_2$ (nanocomposites)	Type C	135	0.12	0.16, 0.18
FL-DAN-$(C11)_2$ (pristine)	Type A	—	—	—
FL-DAN-$(C11)_2$ (nanocomposites)	Type A	161	0.04	0.18, 0.18
FL-DAN-$(C11)_2$ (nanocomposites)	Type B	140	0.09	0.18, 0.19
FL-DAN-$(C11)_2$ (nanocomposites)	Type C	116	0.27	0.18, 0.18

View Article Online

Published on 09 November 2006. Downloaded by National Chiao Tung University on 26/04/2014 08:59:45.

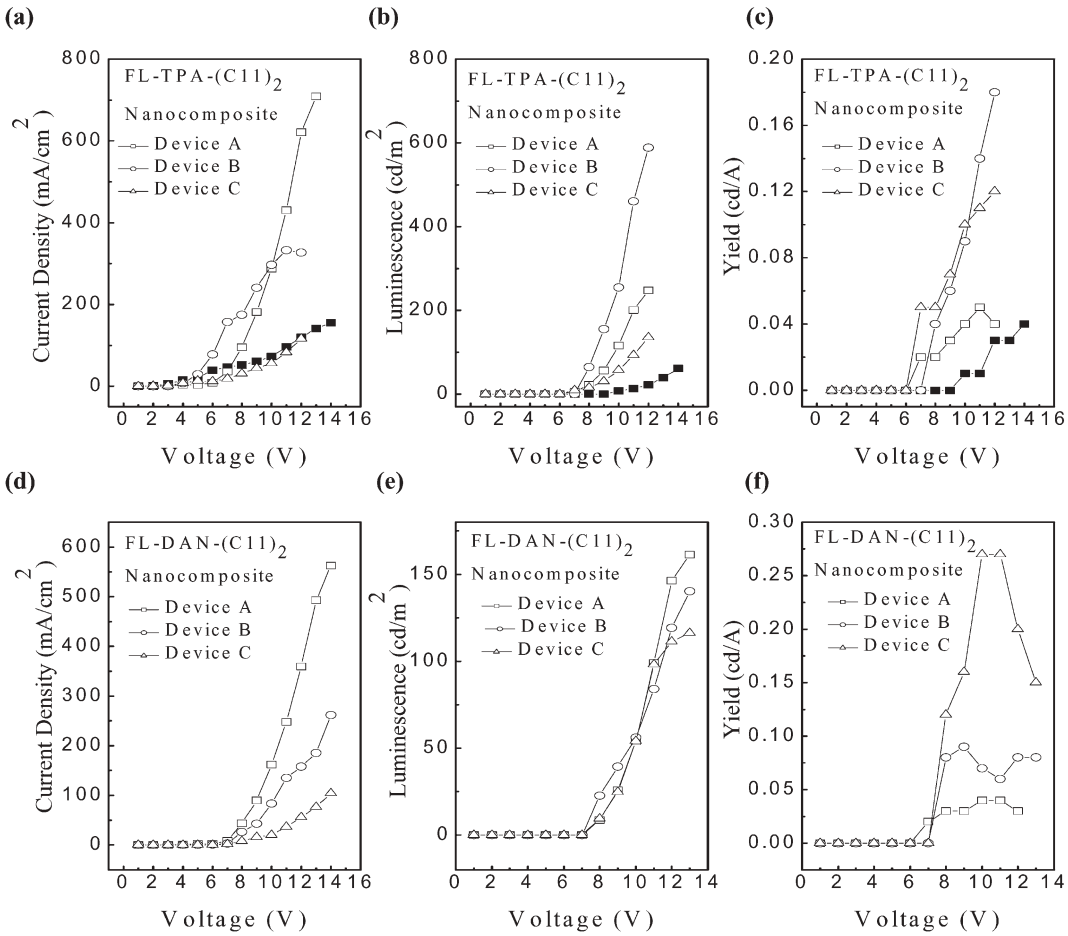

Fig. 6 Comparative (a, d) current density–voltage, (b, e) luminescence–voltage and (c, f) efficiency (yield)–voltage characteristics of various types of LED devices A, B and C (as indicated), fabricated using FL-TPA-$(C11)_2$ and FL-DAN-$(C11)_2$. (Curves for pristine FL-TPA-$(C11)_2$ chromophore are shown as filled squares.)

chromophore amphiphile can not emit light in device A because of the bad film-forming properties. However, its nanocomposite in device A has the luminescence of 161 cd m^{-2} at 13 V and the EL efficiency could reach up to 0.04 cd A^{-1} at 13 V. Introducing either PCF11 (an electron-blocking layer) or TPBI (as hole-blocking layer) would effectively lower the current density and further improve the efficiency by a wide margin (Fig. 6d and f). However, the luminescence of the FL-DAN-$(C11)_2$ nanocomposite seems not to be effectively improved in devices B and C (Fig. 6e); the reason for this may be that the low ionization potential (I_p = 5.87 eV) forms a large energy gap between the EML and the HTL and so it is very difficult for the holes to transport to the EML thus resulting in poor brightness. The introduction of sol–gel co-assembly of silica with the structure-directing chromophore amphiphiles could effectively assist the small molecules in forming well-ordered nanocomposite films, avoiding aggregation shortcomings, and thus can effectively be applied in LED devices.

Gel formation

We further studied the ageing of the nanocomposite gel solutions prepared initially. After more than two weeks of ageing further gelation was observed and a thick fluorescent gel was formed. The photo-images of these gels are shown in Fig. 7a and c insets. These gels show very bright fluorescence under UV light illumination. The gels were dried at room temperature and then calcined at 550 °C for a few hours and the materials formed were characterized by SEM and TEM. The gels of the FL-TPA-$(C11)_2$ and FL-DAN-$(C11)_2$ nanocomposites, after calcination showed worm-like (few hundred nanometers in range) and spherical (sub-micrometer) morphologies, respectively (Fig. 7a and c). Their corresponding transmission electron microscopy images showed patterned and well-ordered arrays of the mesophases as shown in Fig. 7b and d. The FL-DAN-$(C11)_2$ hybrid exhibit exclusively well-defined striped patterns, whereas a hexagonal-like structure is observed for the FL-TPA-$(C11)_2$ hybrid. This shows that the nanocomposites continued to re-organize to produce more stable and well-defined structures over a period of several weeks.

3. Conclusions

In summary, the new blue luminescent fluorene-based amphiphile/silica co-assembled nanocomposite films of two fluorene derivatives FL-TPA-$(C11)_2$ and FL-DAN-$(C11)_2$ have been successfully prepared with enhanced emission; thus we have tried to solve the problem of solid-state quenching of

 This journal is © The Royal Society of Chemistry 2007

View Article Online

Published on 09 November 2006. Downloaded by National Chiao Tung University on 26/04/2014 08:59:45.

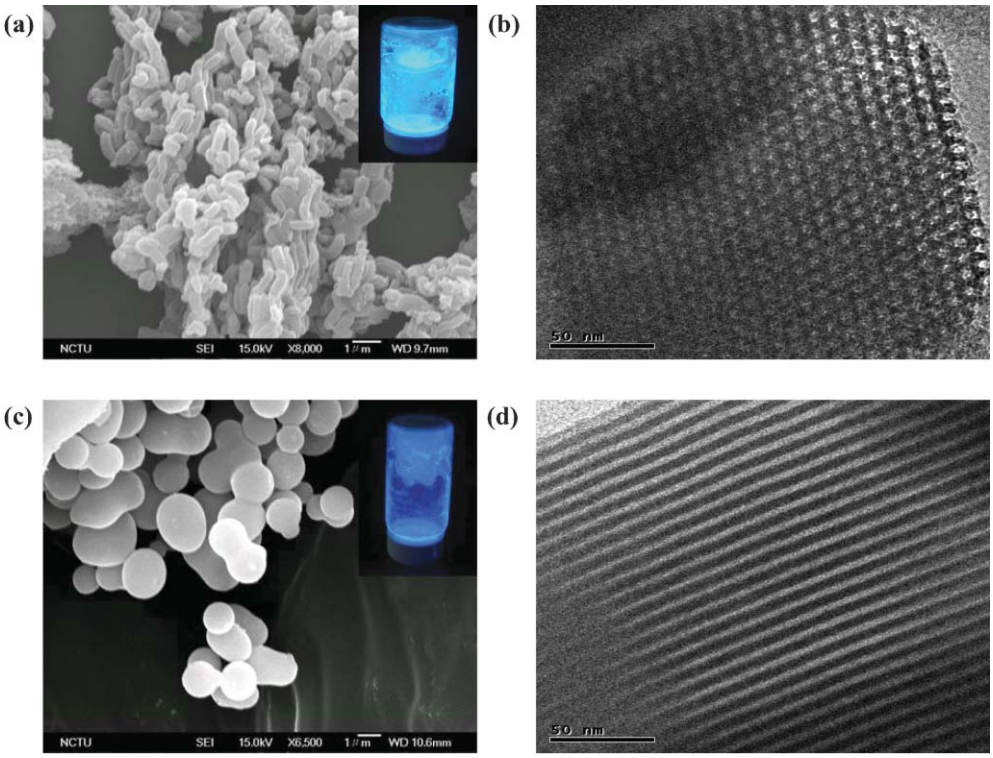

Fig. 7 (a, c) Scanning electron microscopy and (b, d) transmission electron microscopy images of the FL-TPA-$(C11)_2$ and FL-DAN-$(C11)_2$ nanocomposite gels after calcination. Insets: Photoimages of the respective nanocomposite gels under UV light illumination,

the organic chromophores to some extent. The spatial orientation of the chromophore amphiphiles within the mesoscopic structures by sol–gel co-assembly in thin films and the subsequent formation of well ordered chromophore nanopackets in this fashion dramatically impacts the photophysical properties of these materials. Moreover, the chromophore amphiphile/silica co-assembly approach provides a platform to overcome the problem of solid-state quenching in the development of organic light emitting devices with high efficiencies. Different kinds of LED devices have been constructed using these nanocomposite materials in double or multi-layer structures. The maximum luminescence and the yield of FL-TPA-$(C11)_2$ and FL-DAN-$(C11)_2$ were extremely improved by new crosslinkable hole transport layer PCF11 and electron transport layer TPBI materials. The emission curves in EL and film-state PL in both the nanocomposites were very similar, which also strongly suggests that the silica walls defined the chromophore amphiphiles' orientation; avoiding the undesired ill-defined aggregations. These results have demonstrated the fabrication of the LED devices and may become important for future potential in nano-sized LEDs with the simple solution casting process and other organic electronics.

4. Experimental

Characterization techniques

The chemical structures of the chromophore amphiphiles were confirmed by ^{1}H-NMR (300 MHz) and ^{13}C-NMR spectra (75 MHz) on a Varian VXR-300 spectrometer. Images of nanocomposites mounted on carbon tape were acquired on a field-emission scanning electron microscope (JSM-6500 F, JEOL); to enhance the conductivity of the specimen, a layer of platinum was sputtered (duration 30 s, current 30 mA, pressure 4 Pa). TEM micrographs were observed under a JEOL, JEM-2010. UV-Visible spectra were measured with an HP 8453 diode array spectrophotometer. Photoluminescence (PL) spectra were obtained on a Hitachi F-4500 spectrometer, and the PL external efficiency was measured using an integrating sphere. X-Ray diffraction measurements for nanocomposite films were done with a diffractometer (Bede D1 type) with CuKα radiation. Cyclic voltammetric measurements (CV) of the nanocomposites were done in acetonitrile (CH_3CN) with 0.1 M tetrabutylammonium hexafluorophosphate ($TBAPF_6$) as the supporting electrolyte at a scan rate of 50 mV s^{-1}. Platinum wires were used as both the counter and working electrodes, silver/silver ions (Ag in 0.1 M $AgNO_3$ solution, from Bioanalytical Systems, Inc.) were used as the reference electrode, and ferrocene as an internal standard. The corresponding highest-occupied molecular orbital (HOMO) and lowest-unoccupied molecular orbital (LUMO) energy levels were estimated from the onset redox potentials. The structures of isolated chromophore amphiphiles were determined with density-functional theory (DFT) implemented in G03 software package. Geometries of molecules in the ground state were optimized at the B3LYP/3-21G level of theory.

Fabrication and characterization of LEDs

Indium tin oxide (ITO) coated glass substrates were cleaned sequentially in ultrasonic baths of detergent, a

View Article Online

Published on 09 November 2006. Downloaded by National Chiao Tung University on 26/04/2014 08:59:45.

2-propanol–deionized water (1 : 1 by volume) mixture, toluene, deionized water, and acetone. A 50 nm thick hole injection layer of poly(ethylenedioxythiophene) doped with poly(styrene sulfonate) (PEDOT : PSS) was spin-coated on top of the ITO from a 0.7% dispersion in water and dried at 120 °C for 1 h under vacuum. Dilute nanocomposite gel solutions were spin-coated upon the PEDOT layer and dried at room temperature under vacuum for 1 h. The film thickness obtained was about 50 nm and was measured by an Alpha-Step 500 surface profiler (KLA Tencor, Mountain View, CA). The coating thickness of PEDOT and nanocomposite together was about 1000 Å, and the active areas were 0.04 cm^2. The TPBI layer was grown by thermal sublimation under vacuum (3×10^{-6} Torr) and was used as an electron transporting layer, which would also block holes and confine excitons. Finally, 35 nm Ca and 100 nm Al electrodes were thermally evaporated through a shadow mask onto the nanocomposite films using an AUTO 306 vacuum coater (BOC Edwards, Wilmington, MA); typical evaporations were carried out at base pressures lower than 2×10^{-6} Torr. The active area of each EL device was characterized following a standard protocol.

Materials synthesis

Starting materials such as 2,7-dibromofluorene, n-butyllithium, and 2-isopropoxy-4,4,5,5-tetramethyl-1,3,2-dioxaborolane were purchased from Aldrich. All other chemicals, reagents, and solvents were used as received from commercial sources without further purification except tetrahydrofuran (THF) and toluene which weredistilled over sodium–benzophenone. The Suzuki coupling catalyst reagent tetrakis(triphenylphosphine)palladium(0) was purchased from TCI and handled under inert argon atmosphere.

Synthesis and characterization of chromophore amphiphiles FL-TPA-$(C11)_2$ and FL-DAN-$(C11)_2$

Synthesis of fluorene–TPA chromophore amphiphile (FL-TPA-$(C11)_2$). (FL-$(C11)_2$) (**1**): Tetrabutylammonium chloride (TBACl) (0.08 g, 12.34 mmol) was added to 50 wt% NaOH in water and heated at 70 °C. 11-Bromo-1-undecanol (3.1 g, 12.34 mmol) was added after a few minutes. Then 2,7-dibromofluorene (2 g, 6.17 mmol) in THF was slowly added to the mixture, which was stirred and heated at 70 °C overnight. After cooling the reaction mixture to room temperature, THF was removed on rotar. The mixture was poured into water and acidified with dilute HCl and then extracted with ethyl acetate (EA). The organic phase was washed with saturated NaCl, dried over $MgSO_4$ and after removing EA on rotar, the crude product was obtained. The product was purified by column chromatography (SiO_2, 20% EA–hexane) to give 2.6 g (70%) of a highly viscous oil. ^{1}H-NMR (300 MHz, $CDCl_3$, δ (ppm)): 1.23–0.97 (m, 28H, $-CH_2$), 1.50 (m, 4H, $-CH_2$), 1.87 (m, 4H, $-CH_2$), 2.49 (q, 4H, $-CH_2$), 3.57 (t, 4H, $-CH_2$OH), 7.42 (d, 4H, aromatic protons), 7.47 (d, 2H, aromatic protons).

N,*N*-Bis(4-methylphenyl)-*N*-(4-bromophenyl)amine (**2**): A mixture of 4-bromoaniline (5.0 g, 29 mmol), 1-iodotoluene (15.84 g, 72.6 mmol), CuCl (0.143 g, 1.44 mmol), 1,10-phenanthroline (0.262 g, 1.44 mmol) and KOH (13.044 g, 232 mmol) in 40 mL toluene was refluxed at 120 °C with stirring for 12 h. The reactant was cooled to room temperature and then the solvent was stripped off by evaporation. The residue was mixed with 50 mL of water and extracted with 50 mL ethyl acetate. The extracted solution was dried over anhydrous magnesium sulfate. The crude product was isolated by filtration, and further purified by flash chromatography on silica gel, eluting with n-hexane to yield 6.63 g (64.7%) of colorless crystals, mp = 105 °C. ^{1}H-NMR (300 MHz, $CDCl_3$, δ (ppm)): 2.28 (s, 6H, $-CH_3$), 6.8 (d, 2H, aromatic protons), 6.95 (d, 4H, aromatic protons), 7.03 (d, 4H, aromatic protons), 7.24 (d, 2H, aromatic protons). ^{13}C-NMR (75 MHz, $CDCl_3$, δ (ppm)): 147.40, 144.91, 132.86, 131.90, 129.99, 124.66, 123.89, 113.59, 20.83. MS (EI-MS) *m*/*z*: 352.3.

N,*N*-Di(4-methylphenyl)-*N*-[4-(4,4,5,5-tetramethyl-1,3,2-dioxaborolan-2-yl)phenyl]amine (**3**): To a cooled solution (−78 °C) of compound **2** (1 g, 2.8 mmol) in 20 mL dry THF, was added dropwise 3 mL (3.55 mmol) of a 1.6 M solution of n-BuLi in hexane. This mixture was stirred and kept at −78 °C for 1 h. The color of the solution changed from green to white. A solution of 2-isopropoxy-4,4,5,5-tetramethyl-1,3,2-dioxaborolane (0.66 mL, 3.55 mmol) was slowly added over 10 min after which the reaction mixture was allowed to warm to room temperature overnight. The resulting greenish-yellow mixture was extracted with ethyl acetate (3×50 mL), and washed successively with a concentrated sodium carbonate solution and water. The crude product was isolated by filtration, and further purified by flash chromatography on silica gel, eluting with n-hexane to yield 0.48 g (41.0%) of colorless crystals, mp = 156 °C. ^{1}H-NMR (300 MHz, $CDCl_3$, δ (ppm)): 1.36 (s, 12H, $-CH_3$), 2.28 (s, 6H, $-CH_3$), 6.8 (d, 2H, aromatic protons), 6.95 (d, 4H, aromatic protons), 7.03 (d, 4H, aromatic protons), 7.24 (d, 2H, aromatic protons). ^{13}C-NMR (75 MHz, $CDCl_3$, δ (ppm)): 150.96, 144.88, 135.80, 133.10, 129.97, 125.28, 120.52, 83.46, 24.88, 20.90. MS (EI-MS) *m*/*z*: 399.34.

2,7-Di[*N*,*N*-bis(4-methylphenyl)-*N*-(4-phenyl)amine]-9,9-di-(11-hydroxyundecyl)fluorene (FL-DAN-$(C11)_2$) (**4**): Compound **3** (0.72 g, 1.8 mmol), compound **1** (0.6 g, 0.9 mmol) and $Pd(PPh_3)_4$ (0.01 g, 0.01 mmol) were combined in a mixture of toluene and aqueous K_2CO_3 (2 M) in the presence of aliquat 336 as a phase transfer reagent. The solution was first put under the protection of argon and refluxed with vigorous stirring at 85 °C on an oil bath for 1 day. After cooling, the solution was extracted with ethyl acetate and the organic phase was dried over magnesium sulfate, filtered, and rotary evaporated to remove solvent. The crude product was purified by flash chromatography on silica gel, eluting with ethyl acetate–hexane = 1 : 5 to yield 0.80 g (82.3%) of a highly viscous oil. ^{1}H-NMR (300 MHz, $CDCl_3$, δ (ppm)): 0.71–2.05 (m, 20H, fluorene-CH_2–$(CH_2)_m$–CH_2OH, alkyl protons), 2.34 (s, 12H, $-CH_3$), 3.57–3.61 (t, 4H, fluorene-CH_2), 7.03–7.73 (m, 30H, aromatic protons). ^{13}C-NMR (75 MHz, $CDCl_3$, δ (ppm)): 151.50, 145.21, 139.57, 134.64, 132.48, 129.86, 127.54, 124.54, 122.81, 120.74, 119.78, 62.99, 55.11, 40.46, 32.70, 30.01, 29.71, 25.64, 23.78, 20.79). MS (FAB-MS) *m*/*z*: 1049.5. Anal. Calcd for $C_{75}H_{88}N_2O_2$: C, 85.83; N, 2.67; H, 8.45. Found: C, 85.32; N, 2.72; H, 9.04%.

 This journal is © The Royal Society of Chemistry 2007

View Article Online

Published on 09 November 2006. Downloaded by National Chiao Tung University on 26/04/2014 08:59:45.

Synthesis of fluorene–anthracene chromophore amphiphile (FL-DAN-(C11)$_2$). 2-(9-Anthryl)-4,4,5,5-tetramethyl-1,3,2-dioxaborolane (**5**): The procedure for the synthesis of compound **5** was similar to that of compound **3** described above with the starting materials being 9-bromoanthracene (6 g, 23.8 mmol) and 1.6 M n-BuLi (22.3 mL, 35.7 mmol), 2-isopropoxy-4,4,5,5-tetramethyl-1,3,2-dioxaborolane (6 mL, 35.7 mmol). The solution was purified by flash chromatography on silica gel, eluting with ethyl acetate–hexane = 1 : 15 to yield 3.81 g (88%) of white crystals, mp = 156 °C. ^{1}H-NMR (300 MHz, $CDCl_3$, δ (ppm)): 1.57 (s, 12H, $-CH_3$), 7.44–8.47 (m, 9H, aromatic protons). ^{13}C-NMR (75 MHz, CDC_3, δ (ppm)): 135.8, 131.1, 129.4, 128.8, 128.3, 125.8, 124.9, 84.4, 25.2. MS (EI-MS) *m*/*z*: 304.2.

2,7-Di[9-anthryl]-9,9-di(11-hydroxyundecyl)fluorene (FL-DAN-(C11)$_2$) (**6**): The procedures for this synthesis were similar to those for compound **4** described above, with the starting materials of compound **5** (0.55 g, 1.8 mmol), compound **1** (0.6 g, 0.9 mmol), $Pd(PPh_3)_4$ (0.01 g, 0.01 mmol) in a mixture of toluene and aqueous K_2CO_3 (2.0 M) in the presence of aliquat 336 as a phase transfer reagent. The crude product was purified by flash chromatography on silica gel, eluting with ethyl acetate–hexane = 1 : 15 to yield 0.45 g (56.6%) of a brown solid, mp = 156 °C. ^{1}H-NMR (300 MHz, $CDCl_3$, δ (ppm)): 0.93–2.05 (m, 20H, fluorene-CH_2–$(CH_2)_m$–CH_2OH, alkyl protons), 2.34 (s, 12H, $-CH_3$), 3.57–3.61 (t, 4H, fluorene-CH_2), 7.26–8.54 (m, 22H, aromatic protons). ^{13}C-NMR (75 MHz, $CDCl_3$, δ (ppm)): 151.06, 140.33, 137.57, 131.42, 130.32, 130.02, 128.40, 126.86, 126.50, 126.10, 125.31, 125.09, 119.70, 63.05, 55.39, 40.36, 32.74, 29.97, 29.50, 25.65, 24.11. MS (FAB-MS) *m*/*z*: 887.3. Anal. Calcd for $C_{63}H_{70}O_2$: C, 88.06; H, 8.21; O, 3.72 Found: C, 88.38; H, 9.01%.

Acknowledgements

The authors acknowledge the financial support from the National Science Council of the Republic of China (NSC-94-2120-M-009-009) for the research carried out.

References

1 S. A. van Slyke and C. W. Tang, *Appl. Phys. Lett.*, 1987, **51**, 913.
2 J. H. Burroughes, D. C. C. Bradley, A. R. Brown, R. N. Marks, K. Mackay, R. H. Friend, P. L. Burns and A. B. Holme, *Nature*, 1990, **347**, 539.
3 J. G. C. Veinot and T. J. Marks, *Acc. Chem. Res.*, 2005, **38**, 632.
4 Y. T. Tao, C. H. Chuen, C. W. Ko and J. W. Peng, *Chem. Mater.*, 2002, **14**, 4256.
5 I. B. M. Ganschow, G. Schulz-Ekloff and D. Wohrle, *Host–Guest Systems Based on Nanoporous Crystals*, Wiley-VCH Verlag GmbH and Co., Weinheim, 2003.
6 D. W. G. Schulz-Ekloff, B. van Duffel and R. A. Schoonheydt, *Microporous Mesoporous Mater.*, 2002, **51**, 91.
7 C. H. M. Ganschow, E. Kneuper, M. Wark, C. Thiel, G. Schulz-Ekloff, C. Brauchle and D. Wohrle, *Adv. Funct. Mater.*, 2004, **14**, 269.
8 M. W. M. Ganschow, D. Wohrle and G. Schulz-Ekloff, *Angew. Chem., Int. Ed.*, 2000, **39**, 161.
9 P. Innocenzi and G. Brusatin, *Chem. Mater.*, 2001, **13**, 3126.
10 A. Costela, I. Garcia-Moreno, C. Gomez, O. Garcia and R. Sastre, *Appl. Phys. B*, 2002, **75**, 827.
11 C. Peng, H. Zhang, J. Yu, Q. Meng, L. Fu, H. Li, L. Sun and X. Guo, *J. Phys. Chem. B*, 2005, **109**, 15278.
12 Y. Lu, Y. Yang, A. Sellinger, M. Lu, J. Huang, H. Fan, G. Lopez, A. R. Burns, D. Y. Sasaki, J. Shelnutt and C. J. Brinker, *Nature*, 2001, **410**, 913.
13 H. Fan. Y. Lu, A. Stump, S. T. Reed, T. Baer, R. Schunk, V. Perez-Luna, G. P. Lopez and C. J. Brinker, *Nature*, 2000, **405**, 56.
14 C. J. Brinker, Y. Lu, A. Sellinger and H. Fan, *Adv. Mater.*, 1999, **11**, 579.
15 H. Peng, J. Tang, J. Pang, D. Chen, L. Yang, H. S. Ashbaugh, C. J. Brinker, Z. Yang and Y. Lu, *J. Am. Chem. Soc.*, 2005, **127**, 12782.
16 Q. Zhang, K. Ariga, A. Okabe and T. Aida, *J. Am. Chem. Soc.*, 2004, **126**, 988.
17 C. Tsai, S. Tam, Y. Lu and C. J. Brinker, *J. Membr. Sci.*, 2000, **169**, 255.
18 K. Domansky, J. Liu, L.-Q. Wang, M. H. Engelhard and S. Baskaran, *J. Mater. Res.*, 2001, **16**, 2810.
19 P. D. Yang, G. Wirnsberger, H. C. Huang, S. R. Cordero, M. D. McGehee, B. Scott, T. Deng, G. M. Whitesides, B. F. Chmelka, S. K. Buratto and G. D. Stucky, *Science*, 2000, **287**, 465.
20 I. Braun, G. Ihlein, F. Laeri, J. Nockel, G. Schulz-Ekloff, F. Schulth, U. Vietze, O. Weiss and D. Wohrle, *Appl. Phys. B*, 2000, **70**, 335.
21 R. D. Miller, *Science*, 1999, **286**, 421.
22 H. Fan, H. R. Bently, K. R. Kathan, P. Clem, Y. Lu and C. J. Brinker, *J. Non-Cryst. Solids*, 2001, **285**, 79.
23 A. Okabe, T. Fukushima, K. Ariga and T. Aida, *Angew. Chem., Int. Ed.*, 2002, **41**, 3414.
24 P. N. Minoofar, R. Hernandez, S. Chia, B. Dunn, J. I. Zink and A.-C. Franville, *J. Am. Chem. Soc.*, 2002, **124**, 14388.
25 P. N. Minoofar, B. Dunn and J. I. Zink, *J. Am. Chem. Soc.*, 2005, **127**, 2656.
26 C. J. Bhongale and C.-S. Hsu, *Angew. Chem., Int. Ed.*, 2006, **45**, 1404.
27 K. Valle, P. Belleville, F. Pereira and C. Sanchez, *Nat. Mater.*, 2006, **5**, 107.
28 C. T. Kresge, M. E. Leonowicz, W. J. Roth, J. C. Vartuli and J. S. Beck, *Nature*, 1992, **359**, 710.
29 G. V. Rama Rao, G. V. Lopex, J. Bravo, H. Pham, A. K. Datye, H. Xu and T. L. Ward, *Adv. Mater.*, 2002, **14**, 1301.
30 B.-K. An, S.-K. Kwon, S.-D. Jung and S. -Y. Park, *J. Am. Chem. Soc.*, 2001, **124**, 14410.
31 J. Luo, Z. Xie, J. W. Y. Lam, L. Cheng, H. Chen, C. Qiu, H. S. Kwok, X. Zhan, Y. Liu, D. Zhu and B. Z. Tang, *Chem. Commun.*, 2001, 1740.
32 K. Y. Peng, S.-A. Chen, W.-S. Fann, S.-H. Chen and A.-C. Su, *J. Phys. Chem. B*, 2005, **109**, 9368.
33 S. Janietz, D. D. C. Bradley, M. Grell, C. Giebeler, M. Inbasekaran and E. P. Woo, *Appl. Phys. Lett.*, 1998, **73**, 2453.
34 C. Ego, A. C. Grimsdale, F. Uckert, G. Yu, G. Srdanov and K. Mullen, *Adv. Mater.*, 2002, **14**, 809.